

Analysis of *Fermi*-LAT data from Tucana-II: Possible constraints on the Dark Matter models

Pooja Bhattacharjee^{1,2,*}, Sayan Biswas^{3,†}, Pratik Majumdar^{4,‡} and Partha S. Joarder^{1,2,§}
¹ *Department of Physics, Bose Institute, 93/1 A.P.C. Road, Kolkata 700009, India*
² *Centre for Astroparticle Physics and Space Science, Bose Institute, Block EN, Sector V, Salt Lake, Kolkata 700091, India*
³ *Raman Research Institute, C.V. Raman Avenue, Sadashivanagar, Bangalore 560080, India and*
⁴ *Saha Institute of Nuclear Physics, HBNI, 1/AF, Bidhannagar, Kolkata 700064, India*

Tucana-II (Tuc-II), a recently discovered and confirmed Ultra Faint Dwarf Spheroidal galaxy, has a high mass to light ratio as well as a large line-of-sight stellar velocity dispersion, thus making it an ideal candidate for an indirect dark matter search. In this paper, we have analyzed nine years of γ -ray data obtained from the *Fermi*-LAT instrument in the direction of Tuc-II. The fact that no statistically significant γ -ray excess over the background of Tuc-II have been detected from the location of this galaxy. It called for an estimation of the 95% confidence level upper limit of the possible velocity weighted self-annihilation cross-section of the dark matter particles (WIMPs) within Tuc-II by fitting the observed γ -ray flux with the DMFit function. The estimated upper limits of the cross-sections are then compared with similar upper limits of the cross-sections determined by us in three other dwarf galaxies that are considered earlier to be the good dark matter candidates in the literature. We have also compared our results with the cross-sections obtained in various popular theoretical models of the WIMPs to find that our results impose reasonable constraints on the parameter spaces of those models. In the concluding section, we compared our results with the similar results obtained from a combined dSph analysis by the *Fermi*-LAT collaboration as well as the results obtained from the studies of dark matter in the dwarf galaxies by the major ground-based Cherenkov experiments.

Keywords: dark matter, WIMP, ultra faint dwarf spheroidal galaxy, indirect detection.

1. INTRODUCTION

The astrophysical and cosmological observations (e.g. [1, 2]) strongly suggest that some kind of non-luminous and non-baryonic matter, namely the Dark Matter (DM), constitutes almost 75% of the total matter density of the Universe. Regarding the physical nature of such DM, cosmological N-body simulations (e.g. [3, 4]) usually, favor a cold DM (CDM) scenario to explain the formation of the large scale structure of the Universe. In addition, the extension of the Standard Model (SM) of particle physics predicts that CDM could possibly consist of some form of massive, non-baryonic and neutrally charged particles, namely weakly interacting massive particles (WIMPs). WIMPs self pair annihilation (with their masses lying in the range of a few tens of GeV to a few hundreds of TeV) explains the thermal relic abundances (i.e. $\langle \sigma v \rangle \approx 3 \times 10^{-26} \text{ cm}^3 \text{ s}^{-1}$) and are consistent with the currently observed mass density of CDM; e.g.. [5–7]. Such pair-annihilation of the WIMPs may be one of the excellent source of indirect dark matter search [5].

DM pair-annihilation rate and the resulting flux of γ -photons are likely to be proportional to the square of the DM density. The dwarf Spheroidal satellite galaxies (dSph) of the Milky Way (MW) that are the densest DM regions in the galactic halo [8], usually lie away from the direction of the central region of the galaxy. Those dSphs are not too far ($\sim (20 - 200)$ kpc) from the earth [9] and they have low content of gas and dust [10], therefore, making them the potentially excellent targets for an indirect search of DM through the detection of the high energy γ -rays arising from the WIMP annihilations [5]. Over about a decade from now, the Sloan Digital Sky Survey (SDSS) [11, 12], the Panoramic Survey Telescope and Rapid Response System (Pan-STARRS) [13–15], the Dark Energy Survey (DES) [16–19] experiment and certain other surveys by using the Dark Energy Camera at Cerro Tololo [20, 21] have discovered a new class of dSphs, namely the Ultra Faint Dwarf galaxies (UFDs) that have extremely low stellar contents and densities. The UFDs are dominated by old ($\gtrsim 12$ Gyr) stellar populations with large velocity dispersions that possibly

*pooja.bhattacharjee@jcbose.ac.in

†sayan@rri.res.in

‡pratik.majumdar@saha.ac.in

§partha@jcbose.ac.in

indicate the existence of substantial DM components in those UFDs [22]. The recent N-body simulations indicate the existence of huge number of DM sub-halos around the MW's halo [23, 24] and amongst them, few hundreds of these sub-halos might be massive enough to host a dwarf galaxy [23]. With their inferred mass-to-light ratios reaching upto $\sim 3000 M_{\odot}/L_{\odot}$, the UFDs are, therefore, considered to be the best tracers of early DM sub-halos in the Universe as predicted by the Λ CDM cosmological models [23–26]. Recently, a joint DES-*Fermi* collaboration [27] has examined the γ -ray signatures of the WIMP pair-annihilations from about 45 UFDs. The aim of their study was to re-examine the constraints imposed on various theoretical WIMP models by an earlier analysis [5, 28–32] of the γ -ray data from 15 confirmed dSphs performed by the *Fermi* collaboration. At present, two new sky survey programs, namely the Large Synoptic Survey Telescope (LSST) and the Wide-Field Infrared Survey Telescope, are being undertaken/planned to search for more UFD/dSph candidates in the galactic halo and in its neighborhood for a comprehensive study of the DM in the Universe [33].

Motivated by such increasing interest in the indirect search for DM in the UFDs/dSphs, in our previous paper, we (see Ref. [34]; referred hereafter as Paper I) undertook a task of analyzing almost seven years of high energy γ -ray data collected by the *Fermi*-Large Area Telescope (*Fermi*-LAT; sometimes referred simply as the ‘LAT’) in the direction of the particular UFD, namely Triangulum-II (Tri-II). Tri-II was first investigated by the PAN-STARRS 3π program [15]. In paper I, we used the velocity dispersion upper limit of Tri-II obtained from the current estimation of Kirby *et al.*, 2017 [35]. Hence, we derived the 95% confidence level (C.L.) upper limit of photon fluxes (above 100 MeV) as well as the upper limit of $\langle \sigma v \rangle$, as a function of the WIMP mass (m_{DM}), to compare with the ones obtained from a number of theoretical WIMP models. We found that the constraints on the parameter values of various popular WIMP models, as imposed by the LAT-Data from Tri-II, are stronger than the ones imposed by the *Fermi*-data from Ursa Minor (UMi), which was considered in Ref. [5, 28, 29] to be one of the best candidates for DM search amongst the dSphs.

In the present paper, we focus our attention to a recently discovered dwarf satellite, namely Tucana-II (Tuc-II; DES J2251.2-5836) [17, 18, 36]. Tuc-II has already been confirmed to be an UFD (and not a part of any globular cluster) in Ref. [37], principally because of its large projected half light radius, the large velocity dispersion of its member stars, its luminosity-metallicity relation and also because of its large dynamical mass to light ratio, all of which conform to the well-established values of the dwarf galaxies [37–41]. Tuc-II may, as well, be a member of the Magellanic group as it is only about 19 kpc away from the Large Magellanic Cloud (LMC) and about 37 kpc away from the Small Magellanic Cloud (SMC) [17]. The outer region of Tuc-II appears to be in an elongated and distorted shape but the observational noise could, as well, be the reason for such a distortion [17, 42, 43]. Considering various observationally inferred parameter values of Tuc II, Walker *et al.*, 2016 [37]) had suggested that this UFD may not exhibit one of the strongest DM annihilation signal, but may contribute meaningfully to the analysis of stacked data from multiple sources including Tuc-II. Many groups have already studied the Tuc-II in search of dark matter self-annihilation [27, 31, 44, 45].

In this paper, we performed a data analysis of Tuc II with 9 years of *Fermi*-LAT data to search the dark matter and in the absence of any signal we explore the parameter space of the popular DM models. We compare the constraints from Tuc-II with the ones obtained from the analysis of Tri-II and of UMi. Later, we also compare our results on Tuc-II with the ones obtained from the recent DES-discovered UFD, namely Reticulum-II (Ret-II) [17, 18, 46–48]. The *Fermi*-LAT data analysis of Ret-II has already been done in Refs. [27, 31, 45, 49–51] and that seems to exhibit small excess of γ -ray signal of some significance over the background of Ret-II, thus making Ret-II an attractive source to search for the annihilation signals of DM. Our comparison, presented in this paper, have again shown that the constraints imposed by Tuc-II on the popular WIMP models in all the relevant annihilation channels are stronger than the ones expected in the case of Ret-II. For the sake of such study, we here assume a perfect spherical symmetry for Tuc-II and further assume Tuc-II to be in dynamic equilibrium with a negligible contribution to its significantly large, observed line-of-sight stellar velocity dispersion from the possible binary stellar motions in Tuc-II, thus assuming that the gravitational potential of Tuc-II is entirely dominated by DM [37].

The paper is organized along the following line. After stating the observed properties of Tuc-II (in subsection 2.1) that are relevant for our study, we briefly describe the procedure for the analysis of *Fermi*-LAT data from the direction of Tuc-II in subsection 2.2. In subsection 2.3, we estimate the upper limits of the γ -ray flux from Tuc-II by fitting Tuc-II with power-law spectral models with five different power indices. In subsection 3.1, we employ the NFW density profile to model the DM density in UFDs. In that subsection, we also estimate the J-factor and its uncertainties for the possible γ -ray flux arising from the WIMP pair-annihilation in UFDs. In subsection 3.2, we determine the possible upper limit of the γ -ray flux from Tuc-II by using the DMfit Monte Carlo (MC) simulation package [52]. There, we also calculate the possible upper limits of the velocity-averaged pair-annihilation cross-section $\langle \sigma v \rangle$ of the WIMPs for several important pair-annihilation channels and compare those cross-sections with the ones obtained from various theoretical WIMP models. Comparisons of the results from Tuc-II, with the results obtained from Ret-II, UMi, and Tri-II, are also presented in subsection 3.2 of this paper. Finally, a brief discussion of our results presented here *vis-a-vis* the results obtained from UFDs/dSphs with the *Fermi*-LAT and with various ground-based Cherenkov

experiments at higher energies is presented in the concluding section 4.

2. ANALYSIS OF TUC-II

2.1. The relevant observed properties of Tuc-II

A spectroscopic study of a number of stars in the direction of Tuc II was undertaken by Walker *et al.*, 2016 [37] by the use of the Michigan Magellan Fibre System (M2FS). This study [37], along with the previous photometric results on Tuc-II [18, 36], could identify eight probable member stars of Tuc-II that were sufficiently well-resolved to determine an internal velocity dispersion but with large asymmetrical uncertainties, $\sigma_v = 8.6^{+4.4}_{-2.7}$ km s⁻¹ about a mean velocity of $-129.1^{+3.5}_{-3.5}$ km s⁻¹ in the solar rest frame. These and the other important physical properties of Tuc-II that have either been directly observed or have been inferred from the observations of Tuc-II by the authors of Refs. [18, 37, 53], are tabulated in TABLE 1 for later reference.

TABLE 1: Properties of Tuc-II

Property	Value	Reference
Galactic latitude	328.0863°	[18]
Galactic longitude	-52.3248°	[18]
Heliocentric distance ([d])	57 ⁺⁵ ₋₅ kpc	[18]
Metallicity ([Fe/H])	< 0.4	[37]
Projected half light radius (R _h)	165 ^{+27.8} _{-18.5} pc	[18]
Maximum galactocentric angular distance in the sample of the observed member stars in Tuc-II, as measured from the observer's position ([θ _{max}])	0.30°	[53]
Square-root of the luminosity-weighted square of the line-of-sight stellar velocity dispersion (σ _v)	8.6 ^{+4.4} _{-2.7} km s ⁻¹	[37]
Mass within the 2D projected half-light radius ($\frac{M_{1/2}}{M_\odot}$)	2.7 ^{+3.1} _{-1.3} × 10 ⁶	[37]
Dynamical mass-to-light ratio ((M/L _v) _{1/2})	1913 ⁺²²³⁴ ₋₉₅₀ M _⊙ L _⊙ ⁻¹	[37]

In TABLE 1, M_\odot and L_\odot indicate the mass and the total luminosity of the Sun, respectively. Definitions of various other quantities displayed in TABLE 1 are given in [18, 37, 53]; also see Refs.[54–56]. In the subsection 3.1, we will use some of the parameters of Tuc-II enlisted in TABLE 1 to evaluate the so-called J-factor, and hence the γ -ray flux arising from DM annihilation in Tuc-II.

2.2. The *Fermi*-LAT data analysis of Tuc-II

The *Fermi*-LAT is a γ -ray space-based detector that scans the whole sky every 3 hour for an efficient study of the γ -ray sky in an energy range from about 20 MeV to 500 GeV. In this paper, we have used the recent version v10r0p5 of the *Fermi ScienceTools* for the analysis of γ -ray data from Tuc-II. The above version allows us to use the pre-processed PASS 8 dataset of event class 128 that makes use of an improved instrument response function (IRF) P8R2_SOURCE.V6 of the LAT.

We have extracted nearly nine years (i.e. from 2008-05-04 to 2017-10-22) of LAT data in 100 MeV to 300 GeV reconstructed energy range within a 10° radius of interest (ROI) centered on the location of Tuc-II. In the source

TABLE 2: Parameters used in `Science Tools` for Fermi-LAT data analysis

Parameter for data extraction ^a	
Parameter	Value
Source	Tucana-II
Right Ascension (RA)	342.9796
Declination (DEC)	-58.5689
Radius of interest (ROI)	10°
TSTART (MET)	239557418 (2008-08-04 15:43:37.000 UTC)
TSTOP (MET)	530362359 (2017-10-22 10:52:34.000 UTC)
Energy Range	100 MeV - 300 GeV
Fermi Science Tool version	v10r0p5 ^b
gtselect for event selection ^c	
Event class	Source type (128) ^d
Event type	Front+Back (3) ^d
Maximum zenith angle cut	90° ^d
gtmktime for time selection ^e	
Filter applied	(DATA_QUAL > 0)&&(LAT_CONFIG == 1) ^f
ROI-based zenith angle cut	Yes ^f
gtltcube for livetime cube ^g	
Maximum zenith angle cut (z_{cut})	90° ^h
Step size in $\cos(\theta)$	0.025
Pixel size (degrees)	1
gtbin for 3-D (binned) counts map ⁱ	
Size of the X & Y axis (pixels)	140
Image scale (degrees/pixel)	0.1
Coordinate system	Celestial (CEL)
Projection method	AIT
Number of logarithmically uniform energy bins	24
gtexpcube2 for exposure map ^j	
Instrument Response Function (IRF)	P8R2_SOURCE_V6 ^k
Size of the X & Y axis (pixels)	400
Image scale (degrees/pixel)	0.1
Coordinate system	Celestial (CEL)
Projection method	AIT
Number of logarithmically uniform energy bins	24
Diffuse models and Source model XML file ^l	
Galactic diffuse emission model	gll_iem_v06.fits ^m
Extragalactic isotropic diffuse emission model	iso_P8R2_SOURCE_V6_v06.txt ^m
Source catalog	3FGL
Extra radius of interest	5°
Spectral model of Tucana-II	Power law (in Section-2.3) & DMFit Function (in Section-3.2) ⁿ
gtlike for likelihood analysis ^o	
Response functions	P8R2_SOURCE_V6 ^k
Optimizer	NEWMINUIT

^ahttps://fermi.gsfc.nasa.gov/ssc/data/analysis/scitools/extract_latdata.html^b<https://fermi.gsfc.nasa.gov/ssc/data/analysis/software/>^c<https://fermi.gsfc.nasa.gov/ssc/data/analysis/scitools/help/gtselect.txt>^dhttps://fermi.gsfc.nasa.gov/ssc/data/analysis/documentation/Cicerone/Cicerone_Data_Exploration/Data_preparation.html^e<https://fermi.gsfc.nasa.gov/ssc/data/analysis/scitools/help/gtmktime.txt>^fhttps://fermi.gsfc.nasa.gov/ssc/data/analysis/scitools/data_preparation.html^g<https://fermi.gsfc.nasa.gov/ssc/data/analysis/scitools/help/gtltcube.txt>^hhttps://fermi.gsfc.nasa.gov/ssc/data/analysis/documentation/Cicerone/Cicerone_Likelihood/Exposure.htmlⁱ<https://fermi.gsfc.nasa.gov/ssc/data/analysis/scitools/help/gtbin.txt>^j<https://fermi.gsfc.nasa.gov/ssc/data/analysis/scitools/help/gtexpcube2.txt>^khttps://fermi.gsfc.nasa.gov/ssc/data/analysis/documentation/Pass8_usage.html^l<https://fermi.gsfc.nasa.gov/ssc/data/analysis/user/make3FGLxml.py>^m<https://fermi.gsfc.nasa.gov/ssc/data/access/lat/BackgroundModels.html>ⁿhttps://fermi.gsfc.nasa.gov/ssc/data/analysis/scitools/source_models.html^ohttps://fermi.gsfc.nasa.gov/ssc/data/analysis/scitools/binning_likelihood_tutorial.html

model, we have included Tuc-II along with all the point sources from 3FGL catalog within 15° of ROI from the centered position of Tuc-II. We have then performed the binned likelihood analysis on our extracted dataset with the ‘gtlike’ tool [57, 58] by following the instructions given in the `ScienceTools`. The spectral parameters of all the *Fermi*-3FGL sources [59] within $10^\circ \times 10^\circ$ ROI, as well as, the normalization parameters of two diffusion models (i.e. `gll_iem_v06.fits` and `iso_P8R2_SOURCE_V6_v06.txt`) have been left free during the model fitting procedure. The rest of all the background sources within the $15^\circ \times 15^\circ$ ROI have been kept fixed at their values given in the 3FGL catalog [59]. All the required information related to our Fermi-LAT analysis method is mentioned in TABLE 2. In the following, we first model Tuc-II as a source having a power-law spectrum with each of the five different spectral indices and later in section 3.2, we go over to fit the γ -ray spectrum arising from the (assumed) DM-dominated Tuc-II with an MC-simulated DM self-annihilation spectrum generated by the use of the DMFit simulation tool-kit [52].

2.3. Results of the power-law modeling

The form of the differential photon flux for power-law modeling can be expressed as:

$$\frac{dN}{dAdEdt} = N_0 \left(\frac{E}{E_0} \right)^{-\Gamma}, \quad (1)$$

where, dN denotes the number of photons lying between the energy range of E and $E + dE$. dA is the elemental area of detector, in which, photons are incident in time interval, dt . From Eq. (1) N_0 and Γ define the normalization parameter and the spectral index of power-law modeling, respectively, while, E denotes the reconstructed energy. For our analysis we have set the energy scale (E_0) at 100 MeV [5] and dE is varied from 100 MeV to 300 GeV.

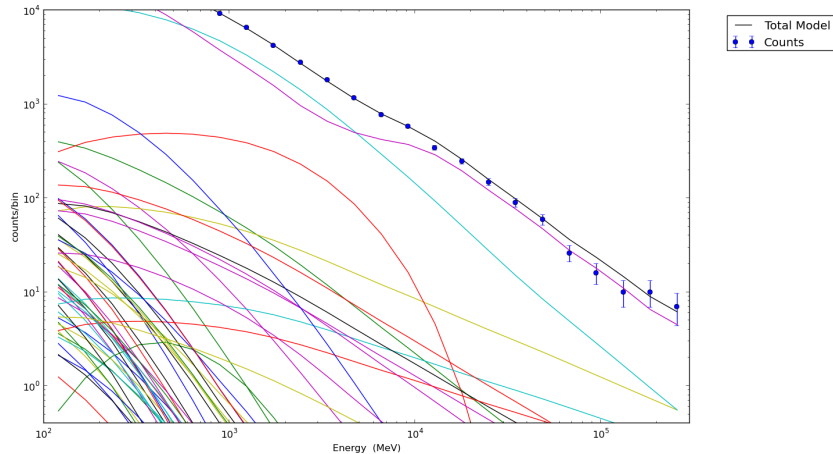
In Fig. 1(a), we display the spectral fit per energy bin of all the sources within the aforesaid ROI, along with the isotropic background component and the galactic diffuse background component. Similarly, Fig. 1(b) displays the corresponding residual plot for all the above sources in the given ROI. The horizontal axes in both these figures indicate the reconstructed energy E of the γ -photons within the chosen range. While the above figures display only the results for modeling Tuc-II with a spectral index $\Gamma = 2$ alone, we have actually repeated this spectral fitting procedure for each of the other values of the spectral index, namely $\Gamma = 1, 1.8, 2.2$ and 2.4 , as well.

The best-fitted values of the N_0 and the Test Statistics (TS) obtained from Tuc-II for each of those spectral indices (Γ) are displayed in TABLE 3. The TS value is the ratio of the maximum likelihoods for two hypothesis, in which, $L_{(\max,1)}$ denotes the maximum likelihood for full model and $L_{(\max,0)}$ refers to the maximum likelihood for null hypothesis. The expression of TS value is $TS = -2 \ln \left(L_{(\max,0)} / L_{(\max,1)} \right)$. It is evident from the TS values that the LAT could not detect excess γ -emission of any significance from the direction of Tuc-II.

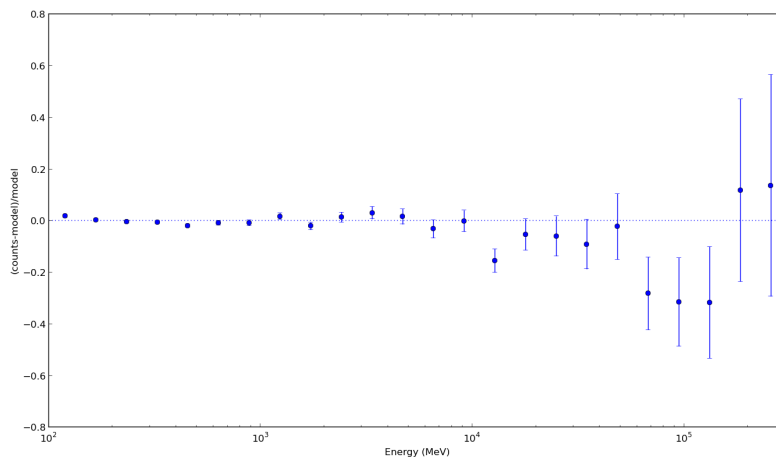
TABLE 3: Best-fitted normalization parameters (N_0) and the TS values obtained from the spectral fittings of the γ -ray flux from Tuc-II with five different spectral indices (Γ).

Spectral Index (Γ)	$N_0 \times 10^{-5}$ ($\text{cm}^{-2} \text{s}^{-1} \text{MeV}^{-1}$)	Test Statistic (TS) value
1	$(7.688 \pm 15.34) \times 10^{-10}$	0.357
1.8	$(8.996 \pm 12.07) \times 10^{-8}$	0.856
2	$(2.381 \pm 2.756) \times 10^{-7}$	1.042
2.2	$(5.065 \pm 5.343) \times 10^{-7}$	1.115
2.4	$(8.540 \pm 9.165) \times 10^{-7}$	0.984

Hence, we calculate the flux upper limit from Tuc-II over the entire reconstructed energy range (0.1 – 300) GeV by the profile likelihood method [60, 61]. During the process of estimating the flux upper limits, all the normalization parameters along with two diffuse components are fitted continuously with the entire dataset until the logarithmic difference of two likelihood functions arrive at the value of 1.35 [5] which corresponds to an one-sided 95% C.L. Next, we have also applied the semi-Bayesian method of Helene [62], as already implemented in the `pyLikelihood` module of `ScienceTools` [63], to obtain a Bayesian γ -ray flux upper limit with 95% C.L. from Tuc-II. These upper limits are displayed in TABLE 4 for each of the spectrum indices (Γ) considered above. In TABLE 4, we note that, the 95% C.L. γ -flux upper limit for $\Gamma = 1$ is almost 20 times lower than the one corresponding to $\Gamma = 2.4$. This result is consistent with our previous work for Tri-II in Paper-I [34], in which, we have also found that the flux upper limit in



(a)



(b)

FIG. 1: Spectral fit to the counts per energy bin (Fig. 1(a)) and the corresponding residual plot (Fig. 1(b)) are displayed for all the sources within the chosen ROI centered on Tuc-II, in which the power-law source-spectral index of Tuc-II is taken as $\Gamma = 2$. In Fig. 1(a), the sky curve displays the best-fit total spectrum, along with the corresponding LAT-observed data points (in blue); the uppermost sky and magenta curves display the galactic diffuse background and the isotropic background component, respectively. The rest of the curves correspond to various point sources other than Tuc-II, lying within the ROI that are not distinctly labeled in Fig. 1(a).

TABLE 4: 95% C.L. γ -ray flux upper limit obtained from the power-law spectral modelings of Tuc-II with five different spectral indices (Γ).

Spectral Index (Γ)	Flux upper limits in 95% C.L. ($\text{cm}^{-2} \text{s}^{-1}$)
1	5.782×10^{-11}
1.8	3.752×10^{-10}
2	5.965×10^{-10}
2.2	8.862×10^{-10}
2.4	1.208×10^{-9}

95 % *C.L.* increased by increasing the spectral indices.

In section 3.2, along with Tuc-II, we have introduced three new dwarf galaxies, namely Tri-II, Ret-II and UMi. For examining the dark matter signature, we have modeled each source with DMFit function implemented in Fermi ScienceTools. We have also followed the same analysis procedure that we have performed for Tuc-II (mentioned in TABLE 2).

3. THE γ -RAY SIGNATURE OF THE WIMP-ANNIHILATIONS IN TUC-II AND THE CONSTRAINTS ON THE DM MODELS

3.1. Estimation of the flux of γ -rays from Tuc-II

The expression for the differential photon flux, arising from WIMP pair-annihilations, in a DM source subtending a solid angle $\Delta\Omega$ at the observer's location is known (e.g. [5, 64]) to be

$$\phi_{\text{WIMP}}(E, \Delta\Omega) = \Phi^{pp}(E) \times J(\Delta\Omega), \quad (2)$$

in which, $\Phi^{pp}(E)$, with the photon energy E , is the *Particle physics factor*; whereas, $J(\Delta\Omega)$ in Eq. (2) is the *Astrophysical factor* or the J-factor. For estimating the γ -ray flux from Tuc-II, we have used the same approach as we used in our paper I [34] but in the following sections, we reproduce brief descriptions of these factors for the sake of completeness.

3.1.1. Particle physics factor

The expression for the particle physics factor that provides information regarding the properties of the initial and the final state particles in various possible WIMP pair-annihilation channels, is given by [5]

$$\Phi^{pp}(E) = \frac{\langle \sigma v \rangle}{8\pi m_{\text{WIMP}}^2} \sum_f \frac{dN_f}{dE} B_f. \quad (3)$$

In Eq. (3), $\langle \sigma v \rangle$ denotes the thermally averaged product of the relative velocity between the WIMPs and their pair-annihilation cross-section [5]; whereas, $\frac{dN_f}{dE}$ and B_f denotes the differential photon spectrum per DM annihilation and the branching ratio of a particular WIMP pair annihilation final state ' f ', respectively.

3.1.2. Astrophysical factor (J-factor)

The expression for the J-factor in Eq. (2) that contains the information regarding the astrophysical properties of the potential DM source (i.e., Tuc-II in the context of this paper), takes the form [5]:

$$J(\Delta\Omega) = J(\lambda, \theta) = 2\pi \int_0^{\theta_{\text{max}}} \sin \theta \int_{\lambda_{\text{min}}}^{\lambda_{\text{max}}} \rho^2(\sqrt{\lambda^2 + d^2 - 2\lambda d \cos \theta}) d\lambda d\theta, \quad (4)$$

Where, $\rho(r)$ is the radial distribution of the DM mass-density in UFDs. In Eq. (4), λ is the line-of-sight (l.o.s) distance, d is the heliocentric distance and θ is the angle between the l.o.s and the center of UFDs, respectively.

Like in Paper-I [34], we use a simple analytical formula for the evaluation of the J-factor in this paper also. This approximate formula was originally provided in Ref. [54] from the solutions of the spherical Jeans' equation in the particular cases of the spherical or the nearly spherical dwarf satellites at sufficiently large distances from the Sun. In our analysis, we have considered the Navarro-Frenk-White (NFW) density profile [65] for modeling the DM distribution in UFDs. This formula is given as

$$J \approx \frac{25}{8G^2} \frac{\sigma_v^4 \theta_{\text{max}}}{dR_h^2}. \quad (5)$$

In Eq. (5), $\theta_{\text{max}} = \arcsin(r_{\text{max}}/d)$; r_{max} is an estimation of the maximum galactocentric distance in the sample of the observed member stars [54] in UFDs. In TABLE 5, we have mentioned all the parameter values required for a numerical estimation of J-factor and its uncertainties for UFDs from Eq. (5). In TABLE 5, the uncertainty in $\log_{10} J$ are calculated from Eq. (5) by using the distribution of σ_v , R_h and d .

TABLE 5: Different parameters to calculate the astrophysical factor (J-factor)

Name	d (kpc)	σ_v (km sec $^{-1}$)	R_h (pc)	θ_{max} (deg)	Median $\log_{10} J$ from Eq. 5 (GeV 2 cm $^{-5}$)	Median $\log_{10} J$ with uncertainties (GeV 2 cm $^{-5}$)
Tuc-II	57 ± 5 [37, 54]	$8.6^{+4.4}_{-2.7}$ [37]	$165^{+27.8}_{-18.5}$ [18]	0.30° [53]	19.14	$19.14^{+0.79}_{-0.68}$
Tri-II	30 ± 2 [15]	< 4.2 [35]	34^{+9}_{-8} [35]	0.15° [66]	< 19.41	
Ret-II	30 ± 3 [54]	3.3 ± 0.7 [46]	55 ± 5 [17, 46]	0.20° [46]	18.53	$18.53^{+0.41}_{-0.39}$
UMi	77 ± 4 [67]	11.61 ± 0.63 [67]	445 ± 44 [67]	0.33° [67]	18.71	$18.71^{+0.15}_{-0.15}$

3.2. Constraints on the DM models

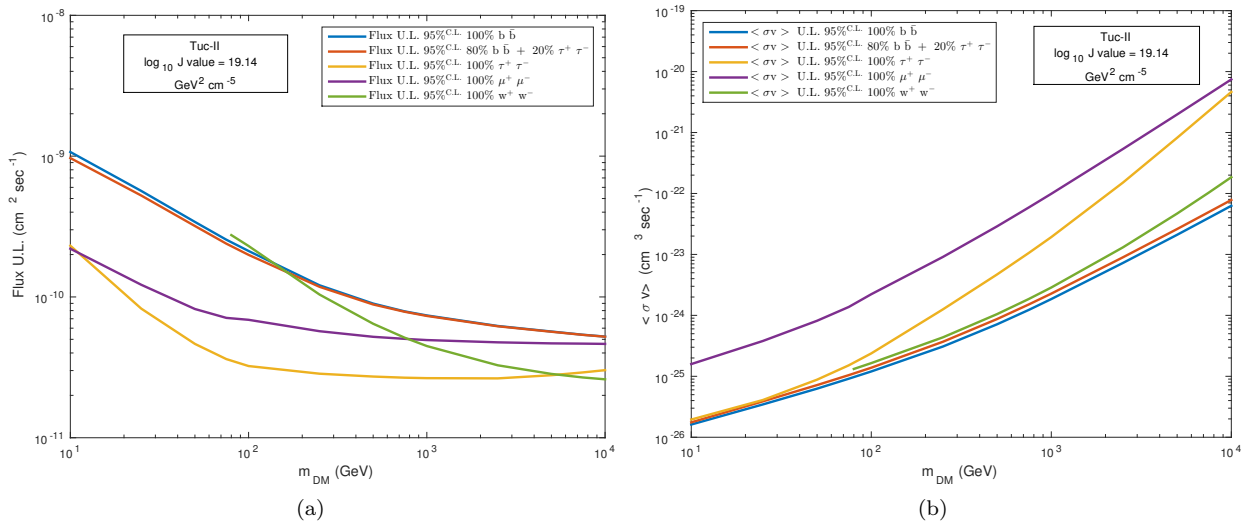
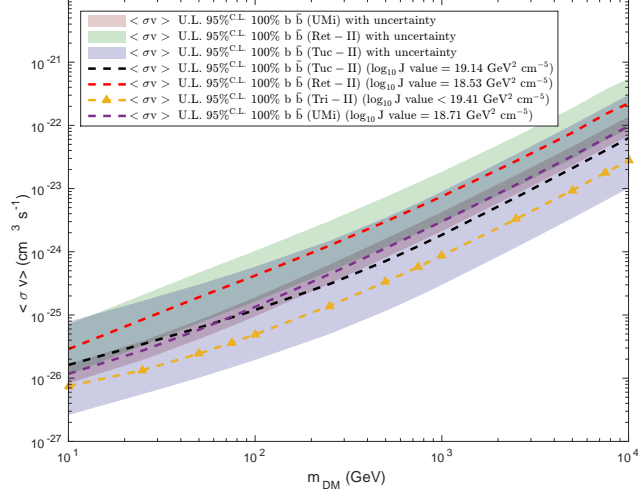


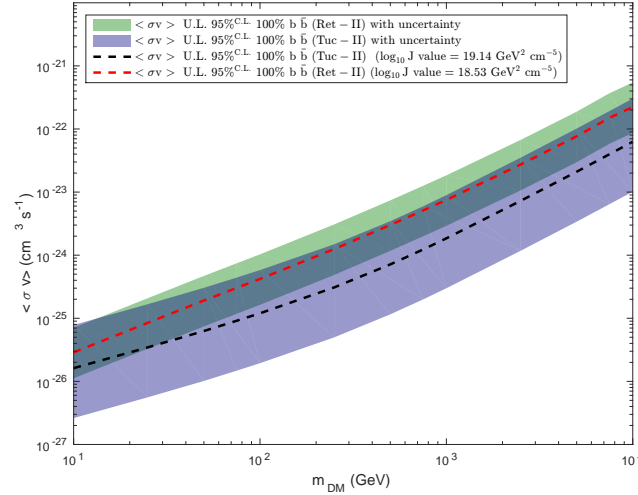
FIG. 2: Variations of (a) the 95% C.L. γ -ray (integral) flux upper limits of Tuc-II and (b) the corresponding pair-annihilation $\langle \sigma v \rangle$ of the WIMPS with their increasing masses (m_{DM}), as estimated for various annihilation final states “f” (indicated in the diagram) by using the DMFit package. Each of these results is estimated for the median J-factor value of Tuc-II (mentioned in TABLE 5).

In this subsection, we have fitted the possible γ -ray flux from Tuc-II in terms of the flux arising out of the pair-annihilation of the WIMPs by employing a full-scale MC simulation package DMFit [52, 68], as implemented in the *ScienceTools*. The DMFit package is based on the particular set of MC simulations of hadronization and/or decay of the annihilation products as used by the DarkSUSY team [52, 68] by means of the Pythia 6.154 [69] event generator. With that package, we have first fitted the LAT-observed γ -ray signal from Tuc-II by semi-Bayesian method [62], as described in subsection 2.2 of this paper. By employing the DMFit package, we could also determine the variation of the thermally averaged pair-annihilation $\langle \sigma v \rangle$ of the WIMPs with the variation of the plausible WIMP masses (m_{DM}), for various important pair-annihilation final states (f), i.e. for each of the possible important channels in which WIMP annihilations might take place to produce γ -rays [7]. For the purpose of this paper, we have considered five such supersymmetry-motivated pair annihilation final states [7], namely 100% $b\bar{b}$, 80% $b\bar{b} + 20\% \tau^+\tau^-$, the 100% $\tau^+\tau^-$, 100% $\mu^+\mu^-$ and 100% W^+W^- , respectively. The variation of such γ -ray flux upper limits for median J-factor value of Tuc-II and the upper limits to their annihilation $\langle \sigma v \rangle$ with increasing WIMP masses are displayed in Fig. 2(a,b), separately for each of the annihilation channels mentioned above.

In Figs. 3(a,b) we have compared the 95% C.L. upper limit of the WIMP annihilation $\langle \sigma v \rangle$ for only $b\bar{b}$ channel obtained by the analysis of nine years of LAT-data of Tuc-II with three other UFDs, namely Tri-II, UMi and Ret-II, respectively. For estimating the 95% C.L. $\langle \sigma v \rangle$ upper limit of these three dwarfs, we have performed the same analysis method that we have applied for Tuc-II (mentioned in TABLE 2).



(a)



(b)

FIG. 3: Variations of (a) 95% C.L. upper limit of the WIMP pair-annihilation $\langle \sigma v \rangle$ with increasing m_{DM} for $b\bar{b}$ annihilation final states of Tuc-II, Tri-II, Ret-II and UMi displayed in $(m_{\text{DM}}, \langle \sigma v \rangle)$ (b) 95% C.L. upper limit of the WIMP pair-annihilation $\langle \sigma v \rangle$ with increasing m_{DM} for $b\bar{b}$ annihilation final states of Tuc-II and Ret-II displayed in $(m_{\text{DM}}, \langle \sigma v \rangle)$. The shaded bands represent the uncertainty in the DM density profiles of UFDs and the dashed line denotes the upper limit of $\langle \sigma v \rangle$ in 95% C.L. corresponds to median J-factor from TABLE 5. In case of Tri-II, we have also displayed the upper limit on $\langle \sigma v \rangle$ that corresponds to the upper limit of its J-factor. The colors and the line-styles of different curves are indicated in the diagram.

In Figs. 3(a,b) the dashed lines correspond to the median value of J-factor, while, the shaded regions depict the range of uncertainty in J-factors of each of the UFDs. These large uncertainty bands represent our inadequate knowledge of the internal structure of UFDs. In case of UFDs, very few numbers of stars have been detected so far which is the main obstacle in understanding the DM distribution in UFDs.

Recent study by Kirby *et. al.*, 2017 ([35]) has observed that the stellar σ_v of Tri-II is inflated by a neighboring binary star and for such scenario they could only estimate σ_v upper limit of Tri-II. So in Fig. 3(a), we have only displayed the $\langle \sigma v \rangle$ upper limit curve of Tri-II for its upper limit of the value of J-factor (i.e. for $\log_{10} J < 19.41$). It may also be of some interest to note that, in case of Ret-II, several recent studies have detected a slight excess in γ -emission [27, 31, 45, 49–51]. Though the significance of excess emission from Ret-II is quite lower than Fermi-LAT’s threshold value for detection, this excess emission is suspected to be the evidence of WIMP annihilation in Ret-II [27, 30, 50, 51].

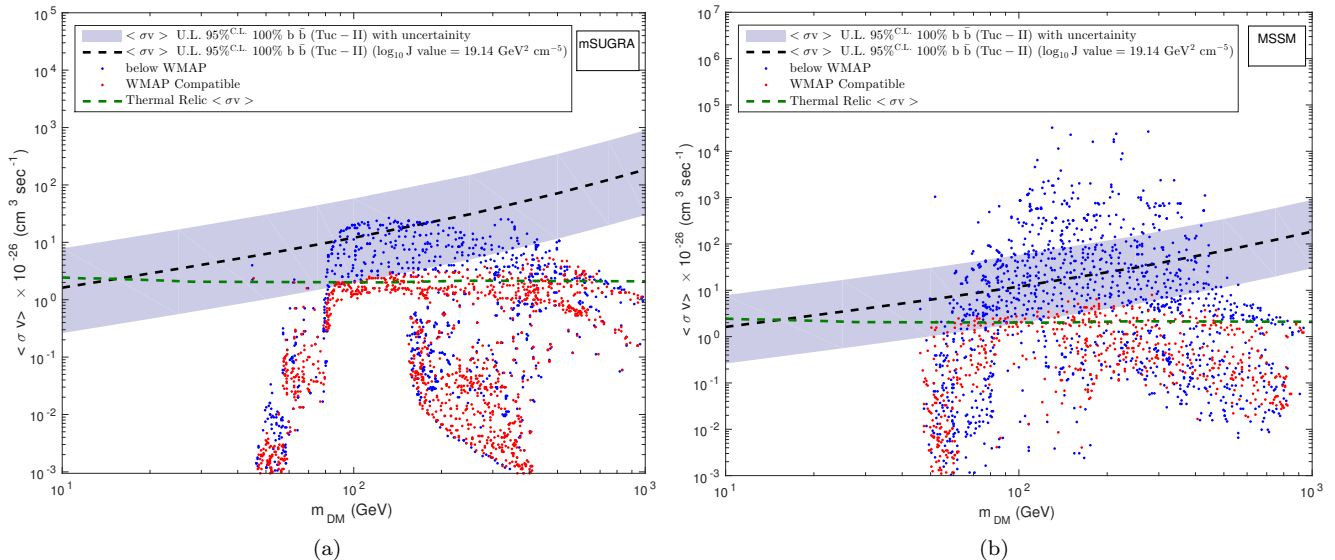


FIG. 4: Variation of 95% C.L. upper limit of the WIMP pair-annihilation $\langle \sigma v \rangle$ with increasing m_{DM} for $b\bar{b}$ annihilation final states of Tuc-II displayed in $(m_{DM}, \langle \sigma v \rangle)$ plane for J-factor with its uncertainties. The shaded band represents the uncertainty in the DM density profiles in the Tuc-II. In the figures, the $\langle \sigma v \rangle$ are compared with points derived from (a) the mSUGRA and of (b) the MSSM models [5]. In those later models, the red points correspond to thermal relic density compatible with the WMAP data. The blue points represent higher $\langle \sigma v \rangle$, and correspondingly lower thermal relic densities, obtained by assuming certain additional nonthermal production mechanisms to contribute to WIMP production, while the WIMPs still comprise all of the DM. In both the figures, we have also overplotted the relic abundance (or thermal) cross section ($2.2 \times 10^{-26} \text{ cm}^3 \text{ s}^{-1}$) estimated by Steigman *et al.*, 2012 [76] and it is displayed as green dashed line.

In Fig. 3(b), we have separately compared the $\langle \sigma v \rangle$ upper limits obtained from Tuc-II with Ret-II along with their uncertainty bands. Compare to Ret-II, Tuc-II indicates the larger uncertainties in DM density profile and but from Fig. 3(b), we could distinctly observe an overlapping region between the Ret-II and Tuc-II in parameter space of $(\langle \sigma v \rangle, m_{DM})$. So, in view of the indirect DM search, it is not possible to firmly favor Tuc-II over Ret-II. For concluding anything in precisely, we need a better understanding of the internal structure of UFDs.

But, from Figs. 3(a,b), it is clearly evident that Tuc-II (with uncertainties band) imposes a comparatively lower limit on the parameter spaces than the ones imposed by Ret-II, UMi, and even by Tri-II. The last one was shown to be a particularly good candidate for constraining the DM models in Paper-I [34]. It is also to be noted that, at about 100 GeV WIMP mass, in 95 % C.L., the lowest limit of $\langle \sigma v \rangle$ upper limit of Tuc-II is lowered by factors of 3, 8 and 5 than the lowest value of $\langle \sigma v \rangle$ upper limit in the cases of Tri-II, Ret-II, and UMi, respectively.

In Figs. 4(a,b) and 5, we have displayed the DMFit-determined 95% C.L. upper limit of the thermally averaged WIMP pair-annihilation $\langle \sigma v \rangle$, as a function of the WIMP mass (m_{DM}), as obtained from the analysis of LAT-data in the direction of Tuc-II for its median J-factor and J-factor uncertainties. These results are then compared with the $\langle \sigma v \rangle$ values obtained for various WIMP masses (m_{DM}) from four theoretical DM models, namely the minimal Supergravity (mSUGRA; in Fig. 4(a)) [70] model, the Minimal Supersymmetric Standard Model (MSSM; in Fig. 4(b)) [71] model, the Anomaly Mediated Supersymmetry Breaking model (AMSB) [72] (in Fig. 4) model and the lightest Kaluza-Klein particle of Universal Extra Dimensions (UED) model [73–75] (in Fig. 5), respectively. Only the $\langle \sigma v \rangle$ upper limit in 100% $b\bar{b}$ annihilation channel has been considered in these figures as they are found to put the most stringent limits on the parameter space of the models. In Figs. 4 and 5, the horizontal dashed green line denotes to the relic abundance (or thermal) cross section estimated by Steigman *et. al.* [76].

From the Figs. 3(a,b), 4(a,b) and 5, it is immediately evident that lowest limit of the shaded band of Tuc-II would

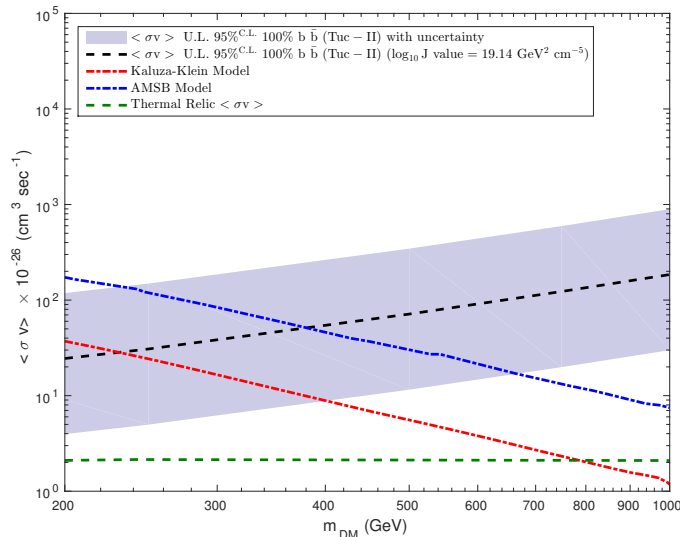


FIG. 5: A comparison between the DMFit-obtained 95% C.L. upper limit of $\langle \sigma v \rangle$ vs. m_{DM} curve from Tuc-II and the theoretical $\langle \sigma v \rangle$ vs. m_{DM} curves obtained from the AMSB and the Kaluza-Klein UED models. The shaded band represents the uncertainty in the DM density profiles in the Tuc-II for $b\bar{b}$ annihilation final states. We have also overplotted the relic abundance (or thermal) cross section ($2.2 \times 10^{-26} \text{ cm}^3 \text{ s}^{-1}$) estimated by Steigman *et al.*, 2012 [76] and it is displayed as green dashed line.

then definitely impose a comparatively tighter constraint on the parameter spaces of the popular theoretical WIMP models than the ones imposed by Ret-II, UMi, and Tri-II. In Figs. 4(a,b) the blue points in both of the models represent the low thermal relic density whereas the red points are consistent with the cosmological thermal relic density. In Fig. 4(b), it is interesting to note that, even for the lowest J-factor of Tuc-II ($\log_{10} J=18.46 \text{ GeV}^2 \text{ cm}^{-5}$), the upper limits of $\langle \sigma v \rangle$ considerably constrain the blue points in MSSM model, while the $\langle \sigma v \rangle$ upper limits corresponds to the highest J-factor ($\log_{10} J=19.93 \text{ GeV}^2 \text{ cm}^{-5}$) of Tuc-II have already begun to constrain the red points in MSSM model. In Fig. 4(a), in the case of the mSUGRA model, the upper limits of $\langle \sigma v \rangle$ for the median J-factor and for the highest J-factor of Tuc-II, only constrain the blue points. By highest and lowest values of J-factor, we want to mean the limiting values of J-factor of Tuc-II (mentioned as a J-factor uncertainty in TABLE-5). Fig. 5 shows that the upper limit of $\langle \sigma v \rangle$ from Tuc-II (with highest $\log_{10} J=19.93 \text{ GeV}^2 \text{ cm}^{-5}$, as determined from Eq. (5) above) disfavors the AMSB and the Kaluza-Klein UED models for masses $< 700 \text{ GeV}$ and $< 400 \text{ GeV}$ respectively, while, on the other hand, for a lowest J-factor of Tuc-II, $\log_{10} J=18.46 \text{ GeV}^2 \text{ cm}^{-5}$ only disfavors the AMSB model for masses below $< 250 \text{ GeV}$.

4. CONCLUSIONS AND DISCUSSION

In this paper, we have analyzed nearly nine years of *Fermi*-LAT γ -ray data from one of the recently discovered UFDs, namely Tuc-II, with the aim of detecting the signatures of self-annihilation of the WIMPs that are usually believed to be the constituent particles of DM within the UFDs/dSphs. No significant γ -ray emission above 100 MeV has, however, been detected from Tuc-II in this study. We have, therefore, determined the 95% C.L. upper limit of the γ -ray flux from Tuc-II that might arise from the pair-annihilation of the WIMPs in Tuc-II. This upper limit has been obtained by fitting *Fermi*-data-points from Tuc-II with the fluxes simulated by using the DMFit MC simulation package for in a quasi-model independent manner. By using Eq. (3), we could then determine the possible upper-limit of the pair-annihilation $\langle \sigma v \rangle$ of the WIMPs in Tuc-II, as the function of WIMP mass, in each of the annihilation channels considered here with an assumption that the entire γ -ray emission arises for particle interaction in that channel only. For estimating the uncertainties in J-factor, we have used a Monte Carlo code. The limiting values of J-factor are determined from Eq. (5), with the inputs being the values of the variables (i.e. σ_v , d and R_h) along with their respective uncertainties. In this paper, we find that, even with a median value of the J-factor determined from an approximate, analytical expression given earlier in the literature, our results could impose more stringent constraints on the theoretical WIMP annihilation $\langle \sigma v \rangle$ obtained in the popular WIMP models than the similar constraints imposed by the observed data from other known dSphs/UFDs, namely the UMi and Ret-II that have

earlier been considered in the literature to be the good candidates for the search of DM.

Recent study of Kirby *et al.*, 2017; [35] observed that a binary star has inflated the previous estimation of σ_v of Tri-II [77] and in their study they only estimated the upper limit of σ_v . With that estimation, in our paper we only present the $\langle \sigma v \rangle$ upper limit of Tri-II for its J-factor upper limit. In case of Ret-II, several studies [27, 31, 45, 49–51] based on Fermi-LAT data analysis have observed an excess emission from the direction of Ret-II and this makes Ret-II as one of the most promising DM-rich UFDs. Hence, our results from Figs. 3(a,b) might create a contradiction with those studies. But, a recent study by Geringer-Sameth *et al.*, 2018 [78] have used a method to identify the exact nature of the excess emission from Ret-II. The analysis by Geringer-Sameth *et al.*, 2018 [78] has given an indication of the existence of possible astrophysical explanations of that excess from Ret-II. From Fig. 3(b) we could also find that it is not possible to strongly favor Tuc-II over Ret-II but our work indicates that by having a adequate knowledge of internal structure, Tuc-II could possibly appear as one of the strongest DM-rich UFDs.

Due to the insufficient kinematics data, the J-factor of Tuc-II comes with a large uncertainty factor. In future with more precise observation of the internal structure of Tuc-II, we could definitely reduce this uncertainty band to a possible single upper limit curve of $\langle \sigma v \rangle$. Previously, several authors have already ([37, 44, 45, 54, 79]) have already estimated the J-factor value of Tuc-II and our estimated J-factor is in good agreement with those values. All of these studies have pointed out the large uncertainty in J-factor of Tuc-II. Despite the large uncertainties in J-factor, our study, presented in this paper, further reveals that Tuc-II can, in fact, impose even better constraints on the theoretical models with a highest and median possible value of J-factor, as obtained from Eq. (5). In the end, to ultimately claim Tuc-II as one of the strongest DM dominated galaxy, we need a more detailed understanding of the DM distribution in Tuc-II.

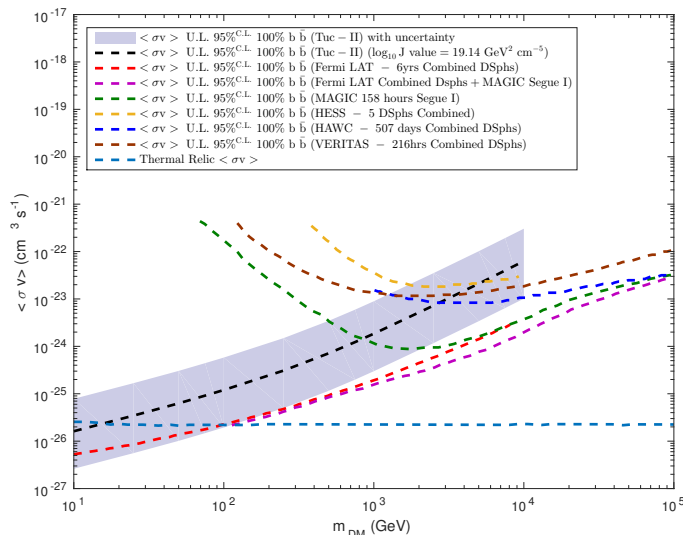


FIG. 6: $\langle \sigma v \rangle$ vs. m_{DM} for $b\bar{b}$ annihilation channel from Tuc-II (obtained in this paper) is shown in comparison with the results obtained from single or combined dSph studies by HESS ([82]), HAWC ([83]), VERITAS ([84]), MAGIC ([81]), *Fermi*-LAT ([80]) and *Fermi*-LAT+MAGIC ([81]) collaboration, respectively. The shaded band represents the uncertainty in the DM density profiles in the Tuc-II. The horizontal dashed sky line corresponds to the relic abundance (or thermal) cross section estimated by Steigman et. al. [76].

In this final section of the paper, we would like to make a comparative study of the upper limits of WIMP pair-annihilation $\langle \sigma v \rangle$, as obtained in this paper, with the $\langle \sigma v \rangle$ obtained from other studies of the dSphs/UFDs. This comparison is displayed in Fig. 6. It includes the results obtained from a combined analysis [80] of 15 dSphs from six years of *Fermi*-LAT data, the results from an analysis [81] of γ -ray data from Segue-I, obtained earlier by using the Major Atmospheric Gamma-ray Imaging Cherenkov Telescopes (MAGIC) alone, as well as, the ones obtained from Segue-I by a joint *Fermi*+MAGIC [81] collaboration. Fig. 6 also includes the results from the analysis [82] of data from a combined study of 5 dSphs by the High Energy Stereoscopic System (H.E.S.S.) of IACT telescopes and the results from the combined study of 15 dSphs [83] by the High Altitude Water Cherenkov (HAWC) gamma-ray observatory and of 4 dSphs [84] by the Very Energetic Radiation Imaging Telescope Array System (VERITAS), as well. In Fig. 6, we find that the joint *Fermi*+MAGIC observations of Segue-I put the best overall limit on the DM annihilation $\langle \sigma v \rangle$ for a wide range of WIMP masses than the limits obtained by various other observations incorporated in that figure. As expected, the combined dSph analysis by the *Fermi*-LAT collaboration also fares well at masses upto about 1 TeV, above which the *Fermi*-LAT begins to suffer from low statistics. The comparison

displayed in Fig. 6 seems to conform to the intuitive belief that the Cherenkov detector arrays should impose stringent limits on the annihilation $\langle \sigma v \rangle$ in the mass range $\gtrsim 10$ TeV, while a joint analysis of spaced-based + ground-based detector is likely to impose the most stringent limits on $\langle \sigma v \rangle$ in the mass range $\lesssim 1$ TeV. It might be interesting to note that the upper-limits on $\langle \sigma v \rangle$ obtained by HAWC and by the *Fermi*+MAGIC collaboration tend to converge in the mass range ≈ 100 TeV, which might indicate that both the IACTs and the Water Cherenkov detectors are becoming competitive in regards to the DM search in the dSphs/UFDs. However, the limiting $\langle \sigma v \rangle$, displayed in Fig. 6, at $\lesssim 1$ TeV WIMP mass range is still about two orders of magnitude away from its relic abundance value. A coordinated effort to combine the data taken from several γ -ray telescopes, as well as, the enhancements of the sensitivity of the Cherenkov telescopes and the improvements of the data analysis techniques of the γ -ray telescopes in general seem, therefore, to be the pressing necessities.

Acknowledgement

We are thankful to the anonymous referee for mentioning some important points which help us to improve our paper a lot. PB is grateful to DST INSPIRE Fellowship Scheme for providing the support for her research. We would like to thank Dr. Stefano Profumo and Dr. Tesla Jeltema of University of California, Santa Cruz, U.S.A., for providing useful guidance in *Fermi*-LAT data analysis. We are particularly grateful to the *Fermi* Science Tools for allowing us to freely access the *Fermi*-LAT data and providing all the needed guidance for our analysis.

-
- [1] E. Komatsu *et al.*, *Astrophys. J. Suppl.* **192**, 18 (2011).
 - [2] P. A. R. Ade *et al.* [Planck Collaboration], *Astron. and Astrophys.* **594**, A13 (2016).
 - [3] J. Diemand *et al.*, *Nature*, **454**, 735 (2008).
 - [4] V. Springel *et al.*, *Mon. Not. R. Astron. Soc.*, **391**, 1685 (2008).
 - [5] A. A. Abdo *et al.*, *Astrophys. J.* **712**, 147 (2010).
 - [6] G. Steigman and M. S. Turner, *Nucl. Phys. B.* **253**, 375 (1985); G. Bertone, D. Hooper and J. Silk, *Phys. Rept.* **405**, 279 (2005).
 - [7] G. Jungman, M. Kamionkowski and K. Griest, *Phys. Rep.* **267**, 195 (1996).
 - [8] A. W. McConnachie, *Astron. J.* **144**, 4 (2012).
 - [9] S. Piatek *et al.*, *Astrophys. J.*, **124**, 3198 (2002).
 - [10] E. K. Grebel *et al.*, *Astron. J.* **125**, 4 (2003).
 - [11] D. G. York *et al.*, *Astron. J.* **120**, 1579 (2000).
 - [12] V. Belokurov *et al.*, *Astrophys. J.* **712**, L103 (2010).
 - [13] N. Kaiser *et al.*, Conference on Survey and Other Telescope Technologies and Discoveries, Waikoloa, Hawaii, August 27-28, (2002), *Proc. SPIE. Int. Soc. Opt. Eng.* **4836**, 154 (2002).
 - [14] B. P. M. Laevens *et al.*, *Astrophys. J.* **813**, 44 (2015).
 - [15] B. P. M. Laevens *et al.*, *Astrophys. J. Lett.* **802**, L18 (2015).
 - [16] T. Abbott *et al.* [Dark Energy Survey], arXiv: 0510346v1 (2005).
 - [17] K. Bechtol *et al.* [Dark Energy Survey], *Astrophys. J.* **807**, 50 (2015).
 - [18] S. E. Kposov *et al.*, *Astrophys. J.* **805**, 130 (2015).
 - [19] D. Kim and H. Jerjen, *Astrophys. J. Lett.* **808**, L39 (2015).
 - [20] D. Kim *et al.*, *Astrophys. J. Lett.* **804**, L44 (2015).
 - [21] N. F. Martin *et al.*, *Astrophys. J. Lett.* **804**, L5 (2015).
 - [22] A. Koch *et al.*, *E Phys. J. web of conferences* **19**, 03002 (2012).
 - [23] M. Kuhlen, **2010**, 162083 (2010).
 - [24] A. Drlica-Wagner, Searching For Dwarf Spheroidal Galaxies and Other Galactic Dark Matter Substructure with the Fermi Large Area Telescope, *Ph.D Thesis*, Stanford University, 2013.
 - [25] V. Belokurov, *New Astron. Rev.* **57**, 100 (2013).
 - [26] D. Kim, Search for Ultra-Faint Milky Way Satellites, *Ph.D Thesis*, Australian National University, 2017.
 - [27] A. Albert *et al.*, *Astrophys. J.* **834**, 110 (2017).
 - [28] M. Ackermann *et al.* [The Fermi-LAT Collaboration], *Phys. Rev. Lett.* **107**, 241302 (2011).
 - [29] M. Ackermann *et al.* [The Fermi-LAT Collaboration], *Phys. Rev. D.* **89**, 04200 (2014).
 - [30] A. Geringer-Sameth *et al.*, *Phys. Rev. D* **91**, 083535 (2015).
 - [31] D. Hooper & T. Linden, *J. Cosmol. Astropart. Phys.* **09**, 016 (2015).
 - [32] M. Ackermann *et al.*, *Phys. Rev. Lett.* **115**, 231301 (2015).
 - [33] C. He *et al.*, *Phys. Rev. D.* **91**, 063515 (2015).
 - [34] S. Biswas *et al.* *J. Cosmol. Astropart. Phys.* **11**, 003 (2017).
 - [35] E. N. Kirby *et al.*, *Astrophys. J.* **838**, 83 (2017).

- [36] A. Drlica-Wagner *et al.* (DES-collaboration), *Astrophys. J.* **813**, 109 (2015).
- [37] M. G. Walker *et al.*, *Astrophys. J.* **819**, 53 (2016).
- [38] G. Gilmore *et al.*, *Nucl. Phys. B.* **173**, 15 (2007)
- [39] E. N. Kirby *et al.*, *Astrophys. J.* **779**, 102 (2013).
- [40] M. L. Mateo, *Astron. and Astrophys.* **36**, 435 (1998); J. S. Gallagher *et al.*, *Astrophys. J.* **588**, 326 (2003); J. Grcevich and M. E. Putman, *Astrophys. J.* **696**, 385 (2009).
- [41] A. P. Ji *et al.*, *Astrophys. J. Lett.* **832**, L3 (2016).
- [42] N. F. Martin *et al.*, *Astrophys. J.* **684**, 1075 (2008).
- [43] R. R. Munoz *et al.*, *Astron. J.* **140**, 138 (2010).
- [44] F. Calore *et al.*, arXiv:1803.05508v2 (2018).
- [45] A. Drlica-Wagner *et al.* [The DES Collaboration], *Astrophys. J. Lett.* **809**, L4 (2015).
- [46] J. D. Simon *et al.*, *Astrophys. J.* **808**, 95 (2015).
- [47] M. G. Walker *et al.*, *Astrophys. J.* **808**, 108 (2015).
- [48] S. E. Koposov *et al.*, *Astrophys. J.* **811**, 62 (2015).
- [49] A. Geringer-Sameth *et al.*, *Phys. Rev. Lett.* **115**, 081101 (2015).
- [50] S. Li *et al.*, *Phys. Rev. D.* **97**, 122001 (2018).
- [51] Y. Zhao, *et al.*, *Chin.Phys. C* **42**, 025102 (2018).
- [52] T. E. Jeltema and S. Profuma, *J. Cosmol. Astropart. Phys.* **11**, 003 (2008).
- [53] A. Chiti *et al.*, *Astrophys. J.* **862**, 1 (2018).
- [54] N. W. Evans, J. L. Sanders, A. Geringer-Sameth, *Phys. Rev. D* **93**, 103512 (2016).
- [55] M. G. Walker *et al.*, *Astrophys. J.* **704**, 1274 (2009).
- [56] J. Wolf *et al.* *Mon. Not. R. Astron. Soc.*, **406**, 1220 (2010).
- [57] W. Cash, *Astrophys. J.* **228**, 939 (1979).
- [58] J. R. Mattox, *et al.*, *Astrophys. J.* **461**, 396 (1996).
- [59] F. Acero, *et al.*, *Astrophys. J. Suupl.* **218**, 23 (2015).
- [60] W. Rolke, A. Lopez, J. Conrad, *Nucl. Instrum. Methods A*, **551**, 493 (2005).
- [61] R. Barbieri, S. Ferrara and C. A. Savay, *Phys. Lett. B* **119**, 343 (1982).
- [62] O. Helene, *Nucl. Instrum. Methods Phys. Res. A*, **300**, 132 (1991).
- [63] A. Loh *et al.*, *Mon. Not. R. Astron. Soc.* **467**, 4462 (2017).
- [64] E. A. Baltz *et al.*, *J. Cosmol. Astropart. Phys.* **07**, 13 (2008).
- [65] J. F. Navarro, C. S. Frenk, S. D. M. White, *Astrophys. J.* **490**, 493 (1997).
- [66] A. Genina and M. Fairbairn, *Mon. Not. R. Astron. Soc.* **463**, 3630 (2016).
- [67] A.B. Pace *et al.*, *Mon. Not. R. Astron. Soc.*, **442**, 1718 (2014).
- [68] P. Gondolo *et al.*, *J. Cosmo Astropart. Phys.* **07**, 008 (2004).
- [69] T. Sjostrand, S. Mrenna, P.Z. Skands, *Comput. Phys. Commun.* **178**, 852 (2008).
- [70] A. H. Chamseddine, R. Arnowitt, P. Nath, *Phys. Rev. Lett.* **49**, 970 (1982).
- [71] D. J. H. Chung *et al.*, *Phys. Rep.* **407**, 1 (2005).
- [72] G. F. Giudice, R. Rattazi, M. A. Luty and H. Murayama, *J. High Energy Phys.* **12**, 027 (1998); L. Randall and R. Sundrum, *Nucl. Phys. B* **557**, 79 (1999).
- [73] H. C. Cheng, J. L. Feng, K. T. Matchev, *Phys. Rev. Lett.* **89**, 211301 (2002).
- [74] G. Servant and T. M. P. Tait, *Nucl. Phys. B* **650**, 391 (2003).
- [75] D. Hooper and S. Profumo, *Phys. Rep.* **453**, 29 (2007).
- [76] G. Steigman *et al.*, *Phys. Rev. D*, **86**, 023506 (2012).
- [77] E. N. Kirby *et al.*, *Astrophys. J. Lett.* **814**, L7 (2015).
- [78] A. Geringer-Sameth *et al.*, arXiv:1807.08740v1 (2018).
- [79] A. B. Pace & L. E. Strigari, arXiv:1802.06811v1 (2018). (2015).
- [80] [Fermi-LAT Collaboration] M. Ackerman *et al.*, *Phys. Rev. Lett.* **115**, 231301 (2015).
- [81] [MAGIC Collaboration] M. L. Ahnen *et al.*, *J. Cosmol. Astropart. Phys.* **2**, 039 (2016).
- [82] [HESS Collaboration] A. Abramowski *et al.*, *Phys. Rev. D* **90**, 112012 (2014).
- [83] [HAWC Collaboration] M. L. Proper *et al.*, ICRC, **LA-UR-15-25701**, 0402 (2015).
- [84] [VERITAS Collaboration] S. Archambaut *et al.*, *Phys. Rev. D* **95**, 082001 (2017).